University of Groningen

Interplay of strain relaxation and chemically induced diffusion barriers

Volkmann, T; Much, F; Biehl, M; Kotrla, M

IMPORTANT NOTE: You are advised to consult the publisher's version (publisher's PDF) if you wish to cite from it. Please check the document version below.

Document Version
Publisher's PDF, also known as Version of record

Publication date:
2005

Link to publication in University of Groningen/UMCG research database

ELSEVIER

Interplay of strain relaxation and chemically induced diffusion barriers: Nanostructure formation in 2D alloys

T. Volkmann [a],*, F. Much [a], M. Biehl [b], M. Kotrla [c]

[a] *Institut für Theoretische Physik und Astrophysik, Universität Würzburg, Am Hubland, 97074 Würzburg, Germany*
[b] *Institute of Mathematics and Computing Science, University of Groningen, P.O. Box 800, 9700 AV Groningen, The Netherlands*
[c] *Institute of Physics, Academy of Sciences of the Czech Republic, Na Slovance 2, 182 21 Prague 8, Czech Republic*

Abstract

We study the formation of nanostructures with alternating stripes composed of bulk-immiscible adsorbates during submonolayer heteroepitaxy. We evaluate the influence of two mechanisms considered in the literature: (i) strain relaxation by alternating arrangement of the adsorbate species and (ii) kinetic segregation due to chemically induced diffusion barriers. A model ternary system of two adsorbates with opposite misfit relative to the substrate, and symmetric binding is investigated by off-lattice as well as lattice kinetic Monte Carlo simulations. We find that neither of the mechanisms (i) or (ii) alone can account for known experimental observations. Rather, a combination of both is needed. We present an off-lattice model which allows for a qualitative reproduction of stripe patterns as well as island ramification in agreement with recent experimental observations for CoAg/Ru(0 0 0 1) [R.Q. Hwang, Phys. Rev. Lett. 76 (1996) 4757]. The quantitative dependencies of stripe width and degree of island ramification on the misfit and interaction strength between the two adsorbate types are presented. Attempts to capture essential features in a simplified lattice gas model show that a detailed incorporation of non-local effects is required.
© 2005 Elsevier B.V. All rights reserved.

Keywords: Non-equilibrium thermodynamics and statistical mechanics; Monte Carlo simulations; Self-assembly; Epitaxy; Alloys

1. Introduction

Heteroepitaxial growth of thin films has been a field of growing interest in recent years [1] as it displays a variety of highly non-trivial phenomena. Among these are, e.g., the self-organized formation of three-dimensional islands, so-called Quantum

---

* Corresponding author. Tel.: +49 931 888 5733; fax: +49 931 888 5141.

E-mail address: volkmann@physik.uni-wuerzburg.de (T. Volkmann).

Dots [2], self-assembly of ordered nanoscale domain patterns [3] or lateral multilayers [4], or the emergence of misfit dislocations [5]. New kinds of materials with unique properties have been fabricated and numerous technical applications are based on hetero-systems. This includes, to name only a few, laser diodes, solar cells, and magnetic or magneto-optical storage devices.

Besides the technological relevance, heteroepitaxy is highly interesting from the theoretical point of view. It provides a workshop to develop and put forward novel approaches and simulation techniques which go beyond the more frequent modeling of homoepitaxial systems [6]. In particular, the correct treatment of kinetic effects in strained systems calls for the development of multiscale techniques. Despite increasing activity in this direction our present understanding of heteroepitaxy on the microscopic level remains rather limited.

In the context of metal epitaxy, the formation of surface alloys is of particular interest. In many cases, adsorbate and substrate intermix and form a thin film of alloy [7]. Another interesting observation is that the deposition of two bulk-immiscible metals, say "A" and "B", upon a suitable substrate "S" can result in the formation of a two-dimensional A–B alloy in the first or several layers of adsorbate. The ordered nanoscale structure formed by alternating domains of material A and B is of particular interest. Such domains are vaguely called stripes or veins, and their formation with a width on the order of nanometers has been observed in a variety of AB/S material systems, including CoAg/Ru(0 0 0 1) [8,9], CoAg/Mo(1 1 0) and FeAg/Mo(1 1 0) [4], CuAg/Ru(0 0 0 1) [10], or PdAu/Ru(0 0 0 1) [11]. Besides the above mentioned stripe substructure, the two component islands in some cases also display dendritic growth [8,9].

In this paper, we investigate microscopic mechanisms relevant for the self-organized formation of nanoscale features in a model ternary AB/S material system during submonolayer growth. Our model system accounts for the key characteristics of the above examples, namely that the atomic size of adsorbate material A is smaller than that of the substrate S whereas that of adsorbate B is larger.

One expects that the presence of both positive and negative misfit in the same heteroepitaxial system will play an important role in the formation and the detailed structure of the growing film. Furthermore, we have to take into account differences in binding energies, and also that the structures are prepared by growth, i.e., under non-equilibrium conditions. On the other hand, interdiffusion of substrate and adsorbates can essentially be neglected in these systems.

Mainly two mechanisms were discussed in the literature in the context of stripe formation

(a) Strain relaxation, see e.g., [4].
As the misfit of A/B particles is negative/positive with respect to the substrate, it is possible to achieve a low effective adsorbate misfit by an alternating arrangement of the species. The essentially geometric effect is illustrated in Fig. 1.

(b) Kinetic segregation, see e.g., [8].
If we assume that the inter-species binding A–B is weaker than that of A–A and B–B, the system tends to separate the elements with a boundary as short as possible. Clearly, in non-equilibrium island growth this cannot be achieved. However, the different binding energies can result in a strong kinetic effect for diffusion along existing edges: a B particle, say, is subject to an extra barrier for diffusion hops from a B to an A domain and vice versa, cf. Fig. 2. Hence, A and B adatoms will preferentially contribute to the growth of domains containing the same species.

Both effects might be sufficient to explain certain aspects of the observed non-equilibrium structures. The main aim of this work is to clarify their role and potential competition in the process of

Fig. 1. Illustration of a ternary system of bigger B-particles (light gray) and smaller A-particles (dark gray) on a substrate (white) of intermediate lattice spacing. The effective misfit of the adsorbate film can be reduced by an alternating arrangement of the species.
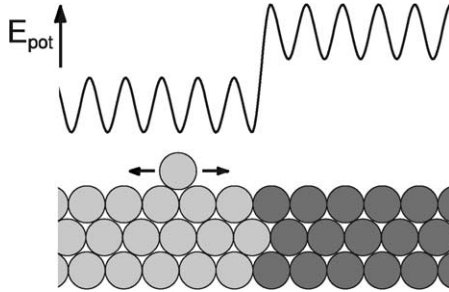
Fig. 2. Illustration of a chemically induced step edge barrier. Lower part: top view on the step edge of an island composed of A-particles (dark gray) and B-particles (light gray). Upper part: schematic diagram of the potential energy experienced by a B-particle diffusing along the step edge.

island and stripe formation. With the help of atomistic simulations, we will demonstrate that both mechanisms are indeed relevant, and that it is their interplay which determines the precise film structures.

The paper is organized as follows. In Section 2, we provide a continuous description of a model ternary system, using an off-lattice simulation model (Section 2.1) which incorporates both misfit-induced strain and binding energy effects. The behavior of the model is studied under both equilibrium (Section 2.2) and non-equilibrium growth conditions (Section 2.3). The influence of misfit and binding energies on the resulting morphologies is discussed. In Section 3, the off-lattice simulations are followed by a description within the framework of the lattice gas method. In order to determine the role of kinetic effects separately from strain effects, a lattice model which incorporates the basic difference in the binding energies of adsorbate species but lacks an explicit representation of strain is introduced (Section 3.1). In Section 3.2 a simplified version of the model which treats both adsorbate species in a symmetric way is investigated and the influence of the binding energies is discussed. In order to compare off-lattice and lattice descriptions, a modified version of the lattice gas model with parameters fitted to characteristic off-lattice diffusion barriers is investigated in Section 3.3. Section 4 summarizes and discusses the obtained results and Section 5 gives a conclusion.

2. Continuous description

2.1. Off-lattice simulation model

In order to simulate heteroepitaxial growth of an adsorbate on a chemically different substrate it is necessary to overcome the limitations of a pre-defined lattice as is discussed, e.g., in [12,13]. For this reason we use a recently introduced off-lattice model [14] which was shown to successfully describe a variety of phenomena observed in heteroepitaxial growth, including dislocation formation, wetting layer and island formation in the Stranski-Krastanov growth mode [14–16]. For a detailed overview, see [13]. In this model two particles which are separated by a *continuous* distance r interact via a simple pair-potential $U(r)$, an example being the Lennard–Jones (LJ) potential

$$U_{LJ}(r) = 4E\left[\left(\frac{\sigma}{r}\right)^{12} - \left(\frac{\sigma}{r}\right)^6\right], \qquad (1)$$

where E determines the depth of the potential and the equilibrium distance between two isolated particles is given by $r_0 = \sqrt[6]{2}\sigma$. By appropriate choice of the parameters E and σ, different material properties may be specified in the model qualitatively. For example, interactions between two substrate or adsorbate particles are governed by the sets $\{E_S, \sigma_S\}$ and $\{E_A, \sigma_A\}$, respectively. To keep the number of parameters small the standard choice $E_{AS} = \sqrt{E_A E_S}$, $\sigma_{AS} = (\sigma_A + \sigma_S)/2$ is used for the interaction between adsorbate and substrate particles. Since the lattice spacing in a Lennard–Jones crystal is proportional to σ [17] the relative lattice misfit ε in the model may directly be controlled by the values of σ_S and σ_A

$$\varepsilon = \frac{\sigma_A - \sigma_S}{\sigma_S}. \qquad (2)$$

In our previous work we have addressed rather fundamental aspects of heteroepitaxial growth [14–16] instead of focusing on specific material properties. In order to save computer time, the simulations therefore were done in $1 + 1$ dimensions. However, phenomena like the formation of alternating vein structures cannot be mapped to $1 + 1$ dimensions. For this reason, we will extend the simulation method to $2 + 1$ dimensions, here.

In order to keep the computational effort acceptable we choose a simple cubic (sc) lattice symmetry for our simulations. The advantage is that due to the lower co-ordination number less particles have to be taken into account for energy calculations than in a close-packed lattice. Note that the majority of the experimental results discussed in Section 1 are for metals grown on substrates with fcc/hcp symmetry. However, this difference should primarily affect the geometry of surface features. We believe that our qualitative conclusions will not depend on this simplification.

In order to stabilize the sc lattice, we adapt the method proposed in [18] and choose

$$V(r) = \left(0.1 + 8\left(\frac{x^2}{r^2} - \frac{1}{2}\right)\left(\frac{y^2}{r^2} - \frac{1}{2}\right)\left(\frac{z^2}{r^2} - \frac{1}{2}\right)\right)U(r) \tag{3}$$

as interaction potential between two particles separated by a distance r. Two kinds of pair-potentials $U(r)$ are used: the LJ potential given by Eq. (1) and the Morse potential

$$U_M(r) = Ee^{a(\sigma-r)}(e^{a(\sigma-r)} - 2). \tag{4}$$

Similar to the LJ potential, the depth of the Morse potential is given by E, and the equilibrium distance between two isolated particles becomes $r_0 = \sigma$. The additional parameter a in Eq. (4) determines the steepness of the Morse potential around its minimum. In our simulations we use $a = 5.0$, 5.5 and 6.0, corresponding to an increase of the steepness. In order to save computer time, $U(r)$ is cut off for particle distances greater than $r_{cut} = 2r_0$ during energy calculations, whereas for the calculation of diffusion barriers the cut-off distance is set to $3r_0$. These simplifications are perfectly justified since both the LJ and the Morse potential decline fast towards zero with increasing particle distance.

In the following we consider two different adsorbate types, called A and B, with negative and positive misfit, respectively, relative to a substrate S. The interaction strength between two substrate particles is given by E_S and $\sigma_S = 1$ whereas E_A, σ_A and E_B, σ_B are chosen for A–A and B–B interactions, respectively. For the interaction between adsorbate particles of type $X \in \{A, B\}$ and

the substrate we use $E_{XS} = \sqrt{E_X E_S}$ and $\sigma_{XS} = (\sigma_X + \sigma_S)/2$ whereas E_{AB} and $\sigma_{AB} = (\sigma_A + \sigma_B)/2$ hold for the interaction between A and B adsorbate particles. The misfit is assumed to be symmetric in the system

$$\sigma_A = 1 - \varepsilon \quad \text{and} \quad \sigma_B = 1 + \varepsilon \tag{5}$$

with $\varepsilon > 0$. Although experimental systems fulfill this symmetry only approximately we do not expect this to be crucial and restrict ourselves to a single parameter ε. The potential depths are chosen in such a way that they meet two demands: on the one hand the ratio between E_S and E_A, E_B is kept fixed for all potentials,

$$E_A = E_B = \frac{1}{6}E_S, \tag{6}$$

and is chosen such that substrate particles are bound much more strongly and thus intermixing of adsorbate and substrate particles is suppressed. On the other hand, in the case of homoepitaxy ($\varepsilon = 0$) the diffusion barrier on plain substrate $E_{a,sub}$ should have roughly the same value for all used potentials to facilitate the comparison of the results. We choose E_S here in such a way that for homoepitaxy $E_{a,sub} \approx 0.37$ eV—a typical value for self-diffusion barriers of metals (see e.g., [19–22]). The resulting E_S for the different potentials are listed in Table 1.

2.2. Equilibrium simulations

In order to determine the influence of misfit and binding energy between A and B particles on the resulting surface patterns, we carry out canonical equilibrium simulations with a fully covered substrate and fixed concentrations η_A, η_B of A and B particles ($\eta_A + \eta_B = 1$). The substrate is prepared as a six-layer-thick crystal with 100×100 particles in each layer and fixed particle positions in the bottom layer. Periodic boundary conditions are ap-

Table 1
The substrate–substrate interaction E_S used in the Lennard–Jones potential (LJ) and the Morse potential with parameter a (M_a)

	LJ	$M_{5.0}$	$M_{5.5}$	$M_{6.0}$
E_S [eV]	3.0	3.0	2.814	2.70

plied in the x- and y-direction. For the range of misfits ε considered in our simulations we do not observe the formation of dislocations even at full coverage. The continuous x- and y-positions of any given adsorbate particle are thus close to the coordinates of a distinct lattice site in a 100×100 square lattice with discrete sites. At the beginning of each simulation run the substrate is randomly covered with adsorbate particles with a given ratio η_A/η_B. Then the system is driven towards thermal equilibrium at temperature T by means of a rejection-free algorithm [23] where A and B particles are exchanged [13,24]. Since, here, we are not interested *how* the system approaches equilibrium we choose a non-local dynamics where the range of particle jumps is unlimited. This yields considerably faster equilibration compared to local Kawasaki-type dynamics [23]. In each event an A particle at site i of the square lattice exchanges its binding site with a B particle at site j according to the rate

$$r_{i \to j} = \exp\left(\frac{\Delta H_i - \Delta H_j}{2 k_B T}\right), \tag{7}$$

where $\Delta H_x = H_x(A) - H_x(B)$ gives the energy difference of the system with site x occupied with an A or B particle. $H_x(A)$ and $H_x(B)$ are calculated in a local way: an A particle is set to site x and all particles within $r_{cut} = 2r_0$ around this site are allowed to relax locally. The local energy is registered as $H_x(A)$. In a similar way we obtain $H_x(B)$. Thus, the rates given by Eq. (7) fulfill the detailed balance condition. To avoid complications in the calculation of the configurational energies $H_x(A)$ and $H_x(B)$ we permit only exchanges between sites i and j which are more than r_{cut} away from each other.

In order to avoid accumulation of artificial strain due to the local relaxation for the calculation of ΔH_x, the system is globally relaxed after a fixed number of simulation steps (here 5000) and all rates are re-evaluated. The system's total energy is registered after each global relaxation. All simulation runs are halted after 20 global relaxation events, i.e., after 10^5 elementary simulation steps.

Fig. 3 shows simulation results for the cubic LJ potential (Eqs. (1) and (3)) for two different values of the misfit ε and various strengths of the A–B interaction E_{AB}. The particle concentrations are $\eta_A = \eta_B = 0.5$. For each parameter set a regular arrangement of alternating A and B stripes may be identified, which are oriented along the $\langle 11 \rangle$ directions, preferentially. As known from other
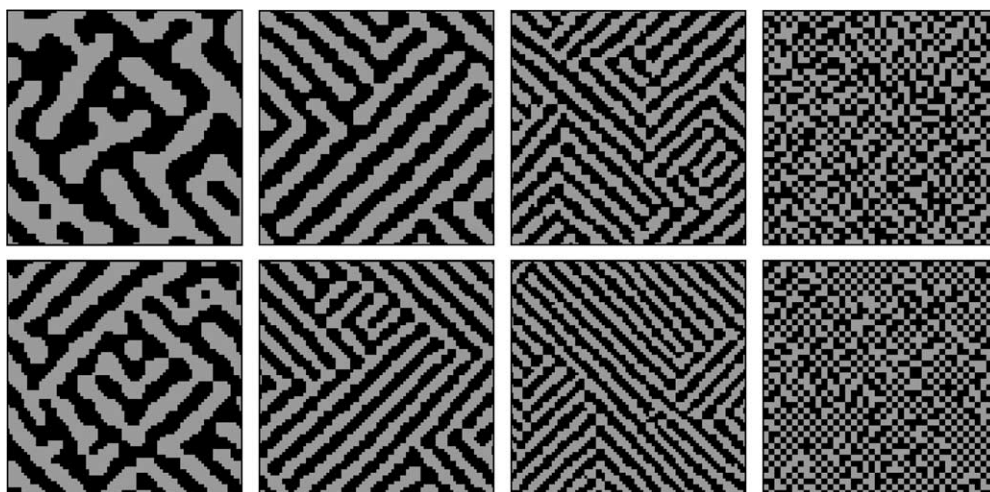

Fig. 3. Snapshots for equilibrium simulations with the Lennard–Jones potential at $T = 250$ K for $E_{AB} = 0.6E_A, 0.8E_A, 0.9E_A, 1.0E_A$ (from left to right) and $\varepsilon = 4.5\%$ (top), $\varepsilon = 5.5\%$ (bottom). The particle concentrations are $\eta_A = \eta_B = 0.5$. The panels for $E_{AB} = 1.0E_A$ show 40×40 sections, the remaining panels 80×80 sections of the 100×100 system. The bigger B particles appear in light gray.

atomistic models with size mismatch [7,27] these regular patterns arise from the competition between binding energy of the particles and strain energy. As one can see in Fig. 3, with increasing E_{AB} and increasing ε the stripes become thinner and more regular in size and shape. For the case $E_{AB} = E_A = E_B$ the system approaches a checkered state, i.e., a stripe width of one. The alignment of the stripes along the $\langle 1\,1 \rangle$ directions is due to the cubic symmetry of the potential: both particle types try to reach their preferred stripe width in each lattice direction (x and y). Note, that the used cubic form of the potential (Eq. (3)) has only a weak interaction in the $\langle 1\,1 \rangle$ direction [13].

Fig. 4(a) shows the width l of A and B stripes for $E_{AB} = 0.6E_A$ in dependence of the misfit. Since the concentrations of A and B particles are equal the stripes have about the same width for both adsorbate types. For very small misfits the alignment of the stripes along $\langle 1\,1 \rangle$ vanishes in favor of a $\langle 1\,0 \rangle$ orientation which decreases the interfacial energy between A and B regions. This process is reflected in the large deviations of the stripe width at $\varepsilon = 0.01$ in Fig. 4(a).

The situation changes completely for $\eta_A \neq \eta_B$. As Fig. 4(b) shows for $E_{AB} = 0.9E_A$ and $\varepsilon = 5\%$,

the stripe width increases with increasing concentration of the particle type. It is noticeable that the bigger B particles form thinner stripes at high B concentration than the smaller A particles at high A concentration. This is due to the asymmetric pair-potential, which is steeper in compression than in tension and thus (compressed) B stripes are slightly more restricted in their width than A stripes.

With otherwise unchanged parameters we performed additional simulations for the Morse potential with $a = 6.0$, which is steeper in both—compression and tension—than the LJ potential used before. However, LJ and Morse potential yield quite similar results: again the competition between strain and binding energy causes alternating stripes of decreasing width with increasing ε. Due to the cubic symmetry the stripes are again solely aligned in the $\langle 1\,1 \rangle$ direction, only for very small misfits stripes can also be found along $\langle 1\,0 \rangle$.

As Fig. 5 points out, the main difference one observes is that for the same misfit and $E_{AB} \leqslant 0.6E_A$ the stripes for the Morse potential are systematically thicker, whereas at higher values of E_{AB} the mean stripe width is nearly identical for both potentials at a given misfit. However, even at
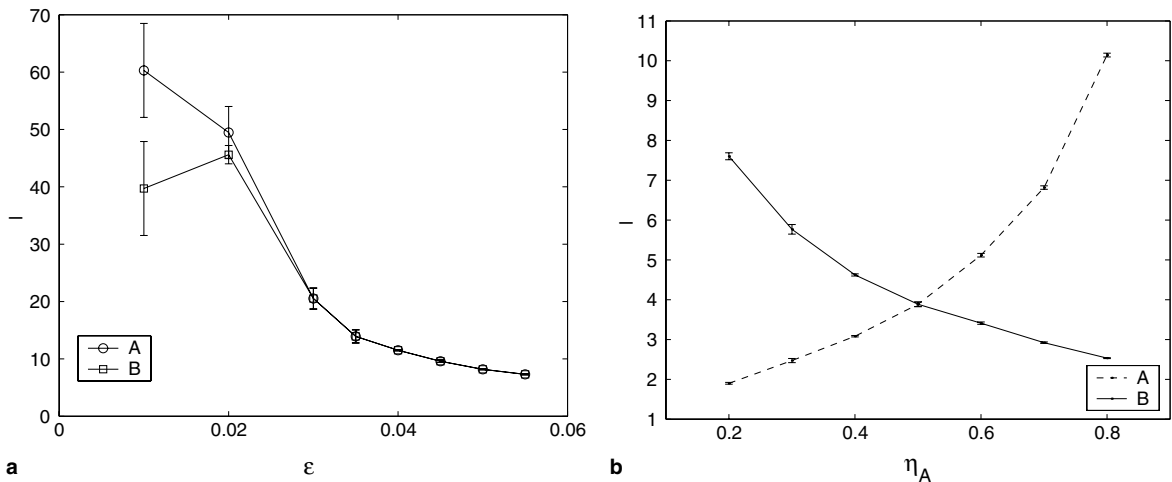

Fig. 4. Equilibrium simulations with the Lennard–Jones potential at $T = 250$ K. (a) Dependence of the stripe width l on the misfit ε for $E_{AB} = 0.6E_A$ and particle concentrations $\eta_A = \eta_B = 0.5$. Due to the onset of stripe formation along $\langle 1\,0 \rangle$ the determination of the stripe width becomes inaccurate for misfits $\varepsilon \leqslant 0.01$. (b) Dependence of the stripe width l on the A particle concentration η_A ($\eta_B = 1 - \eta_A$, consequently) for $\varepsilon = 5\%$ and $E_{AB} = 0.9E_A$. Each value is obtained by averaging over three independent simulation runs.
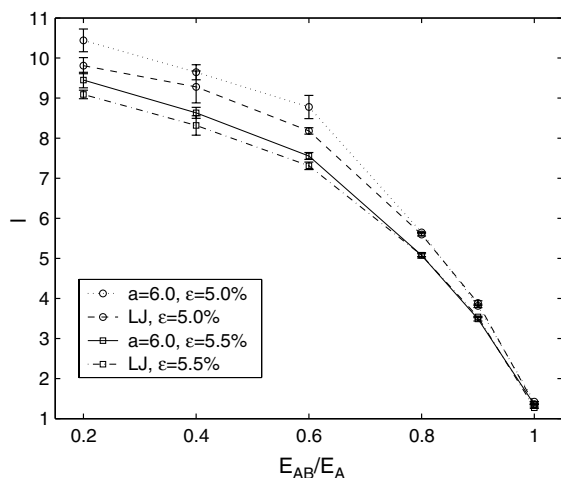
Fig. 5. Equilibrium simulations at $T = 250$ K. Shown is the width l of B stripes as a function of E_{AB} for the Lennard–Jones and the Morse ($a = 6.0$) potential for different values of ε. Each data point is obtained by averaging over three independent simulation runs.

values $E_{AB} \leqslant 0.6E_A$ the deviations are small compared to the influence of the particle concentration on the stripe width.

The equilibrium simulations with the off-lattice model show that the combination of the binding energy $E_{AB} > 0$ between A and B particles together with the misfit $\varepsilon > 0$ yields regular patterns of alternating stripes. This morphology is produced for a wide range of parameters and independently of the details of the interactions. The width of the stripes is controlled by the value of ε together with the binding energy.

2.3. Island morphology under non-equilibrium conditions

In the following we will address the question whether the evolution of a system, which is governed by a competition between strain and binding energy, under non-equilibrium growth conditions yields similar morphologies as the ones observed in thermal equilibrium. Therefore, we perform kinetic Monte Carlo (KMC) simulations with an increasing number of particles. Two microscopic processes are taken into account: (i) random deposition of adsorbate particles and (ii) diffusion of

adatoms on the surface. Since desorption of adsorbate particles is negligible in the considered temperature regime, it is not included in our simulations. Growth takes place on a 100×100 substrate of six layers height with fixed bottom layer and periodic boundary conditions in x- and y-direction. For all simulation runs the deposition rate for both types of particles is set to 5×10^{-3} ML s^{-1}. Thus, the resulting overall deposition rate is $R_d = 10^{-2}$ ML s^{-1}. The simulations are halted when half the substrate is covered with adsorbate particles. Since we are only interested in the submonolayer regime we disregard second layer nucleation, i.e., particles which are deposited onto other particles will be ignored. Jumps of particles onto others are suppressed for the same reason. The diffusion of adatoms is described by thermally activated hopping processes between neighboring binding sites with Arrhenius rates [23]

$$R = v \exp\left(-\frac{E_a}{k_B T}\right). \tag{8}$$

We use $v = 10^{12}$ s^{-1} as common attempt frequency for all diffusion events. The activation energy E_a for a diffusion jump of a particle between two binding sites is given by $E_a = E_t - E_b$ where E_t and E_b are the potential energies of the particle at the transition state and the initial binding site, respectively. Since in the considered misfit regime dislocations do not appear, E_b can be determined rather easily by placing the particle on the perfect square lattice site and subsequent relaxation with respect to the precise, continuous particle positions [13]. The calculation of E_t implies searching for a first order saddle point in the potential energy surface (PES) generated by the superposition of all pair-interactions according to Eq. (3) [13]. This is achieved by an iterative algorithm, the so-called activation-relaxation technique (ART) [28,29].

As interaction strength between A and B particles we choose

$$E_{AB} = 0.6E_A, \tag{9}$$

which—under equilibrium conditions—leads to the formation of rather thick stripes and for which the influence of the misfit should be clearly observable. On the basis of the equilibrium simulation results, we expect also a noticeable dependence

on the choice of the potential for this interaction strength. Note that $E_A = E_B$ are given according to Eq. (6) and E_S is specified in Table 1 for the different potentials.

This choice of the potential depth yields a higher barrier for edge diffusion than for diffusion on plain substrate in our simulations. However, the barrier for edge diffusion is still smaller than that for detachment from the edge. So particles attached to an island edge are more likely to diffuse there than to detach. This is of particular importance since we focus here on phenomena, where edge diffusion is supposed to have a strong impact (cf. Section 1 and [8,9]). Note also that for the cubic lattice (Eq. (3)) diagonal diffusion jumps can be neglected since they imply traversing a maximum in the PES [13]. The kinetic Monte Carlo simulations are carried out following the standard scheme where in each Monte Carlo step an event k (deposition or diffusion) is chosen according to its rate R_k and performed [23]. The crystal is then locally relaxed around the location of the event and the rates for all events affected by this relaxation are re-evaluated. The system time is incremented by an interval τ which is chosen from an exponential distribution [23]. Similar to the equilibrium simulations, a relaxation of the entire system is performed after 4×10^5 steps in order to avoid strain accumulation.

We present now results on the influence of the misfit and the used potential at a temperature $T = 500$ K. Comparative simulation runs showed that under the same growth conditions both particle types form compact, rectangular islands if they are deposited alone onto the substrate. We also observed for the B particles with positive misfit that an island which becomes larger than a critical island size splits up into smaller islands. This can be understood as relaxation of the accumulated compressive strain in the island. Note that a similar effect is observed experimentally for Cu/Ni(1 1 0) where copper islands undergo a shape transition when they exceed a critical island size [30].

In the case of co-deposition, we observe a completely different situation: Fig. 6 shows snapshots of simulation runs for the Morse potential (Eq. (4)) for various values of a and ε. These structures are exemplary for all simulation results: the B particles (shown in light gray) assemble into a few big clusters. With increasing misfit the branches of these clusters become thinner and of more uniform width. The A particles surround these branches without showing a similar shape. It is also seen from Fig. 6 that with increasing misfit the ramification of the structure as a whole increases. This is clearly related to the restricted width of the B stripes: a B particle rather attaches to the thin end of a stripe. This implies that thinner stripes of material B (light gray) grow outwards faster, leading to increasing ramification of the structure.

At a given misfit the B branches are the thinner the smaller the value of a in the Morse potential is. Consequently, at a given misfit the island-ramification is more pronounced for $a = 5.0$ than for $a = 6.0$. This is in agreement with the equilibrium simulations where a steeper potential yields thicker stripes.

In order to quantify the observations we calculate for each connected cluster of B particles the ratio Λ between its perimeter length and its volume. This is done by counting the number of perimeter particles together with the total number of particles in the same cluster. We take only the *backbone* of the structures into account and neglect smaller clusters (<700 particles).

The ratio Λ is a measure for the average thickness of the cluster, see Fig. 7(a). For example, for a rather thin cluster most of its particles sit at the edge and therefore Λ should be close to 1, whereas Λ should decrease if the cluster becomes more compact. In addition, we measure the species-independent quantity Γ, which is given by the number of particles in the system with less then 4 nearest neighbors, divided by the square root of the total number of adatoms. Γ provides a measure for the length of the structure's perimeter and therefore the ramification, see Fig. 7(b). A single perfect quadratic island on the substrate corresponds to $\Gamma \approx 4$, whereas larger values of Γ indicate roughening of the island shape. The correlation between Λ and Γ is clearly observable for all used potentials: Λ increases with increasing misfit indicating thinner B clusters. Simultaneously the ramification increases. The formation of B branches of well-defined thickness is a common phenomenon for the used pair-potentials.
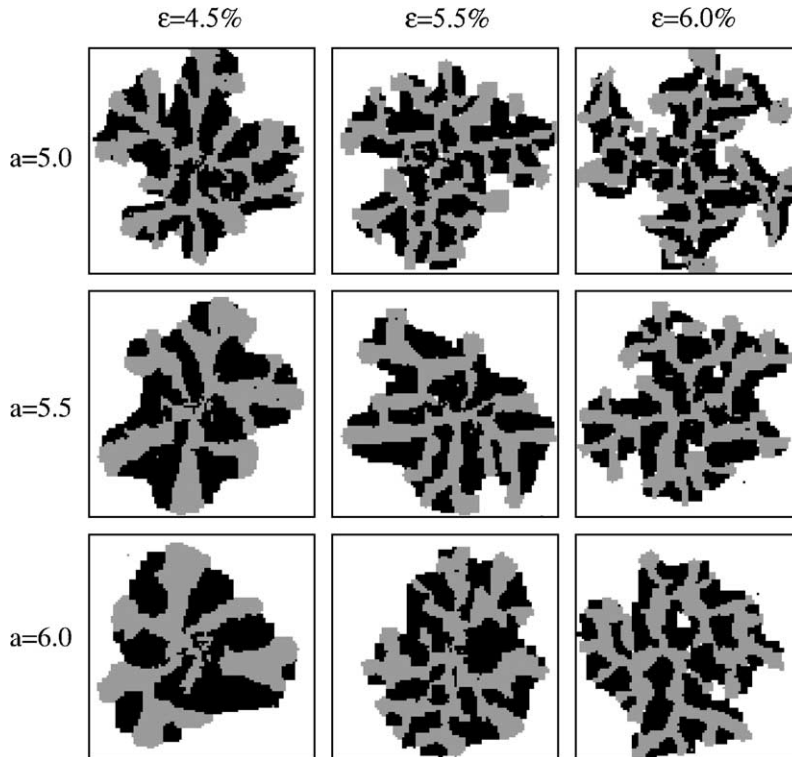
Fig. 6. Exemplary surface configurations obtained by KMC simulations with the Morse potential (Eq. (4)) for various values of the parameter *a* and misfit ε. The bigger B particles are shown in light gray.
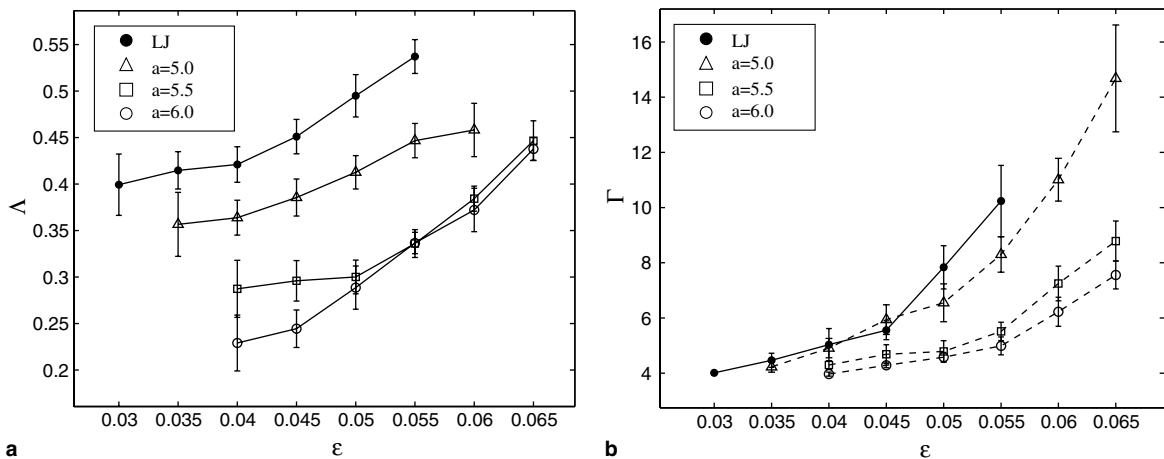

Fig. 7. (a) Ratio *Λ* between perimeter particles and total number of particles in the big B clusters for the used potentials. (b) The number of perimeter particles divided by the square root of deposited particles *Γ* versus ε. Each value is obtained by averaging over ten independent simulation runs. The errorbars are given by the standard deviation.

One might suspect that the observed ramification of the islands is due to temperature effects, only: i.e., the used temperature may be high enough for the formation of cubic clusters of a single

species, but enlarged edge diffusion barriers in the case of mixed deposition might cause dendritic growth at the same temperature.

In order to investigate the temperature dependence of the island morphologies we performed simulations for temperatures between 400 K and 550 K using the LJ potential with $\varepsilon = 5.0\%$ and the Morse potential with $a = 6.0$ and $\varepsilon = 6.5\%$. For the given parameters, strongly ramified islands grow at $T = 500$ K. At low temperatures we observe multiple islands due to the reduced diffusion length. They exhibit frayed edges and rather thin and disordered B stripes. With increasing temperature the B stripes become wider and more regular in shape, the island edges become smoother. The observations are reflected in the temperature dependence of Λ and Γ as shown in Fig. 8(a) and (b). We stress that the ramification Γ does not decrease monotonously with increasing temperature (as one might expect). For both potentials it exhibits a minimum at $T \approx 475$ K and then slowly increases with T for higher temperatures. This observation clearly rules out that the observed ramification is merely an artefact of the low growth temperature.

The enhanced mobility of the particles causes a more distinct separation of the two particle types, resulting in more regular B stripes. As Fig. 8(a) shows the width of the B stripes approaches a con-

stant value for the high temperature region. Furthermore, we observed that for high enough temperatures nearly all B clusters are aligned in the $\langle 1\,1 \rangle$ directions in order to achieve the energetically most favorable arrangement of particles like in the equilibrium simulations (see [13]).

The question now is in which way the observed branches are related to the stripe structures found in the equilibrium simulations. Fig. 9(a) shows the potential energy for a B particle diffusing near an A–B interface for $\varepsilon = 4\%$ and $E_{AB} = 0.6E_A$. The weaker A–B interaction causes an extra step edge diffusion barrier for the jump from the B to the A region. This can be more clearly seen in Fig. 9(b) where the diffusion barrier for a jump to the left is plotted versus the particle position. The diffusion barriers are given by the energy difference between the corresponding transition state energy and the binding energy. A similar plot is obtained for the rightward diffusion jumps of an A particle. As already mentioned in Section 1 the enhanced diffusion barrier at the A–B interface is believed to favor the formation of alternating stripes.

In the following section, we discuss, by means of a lattice gas model, how such a diffusion barrier influences the multi-component growth. Of special interest is the question, whether the stripe formation and the island morphology, as observed in our off-lattice simulations, can be explained in a
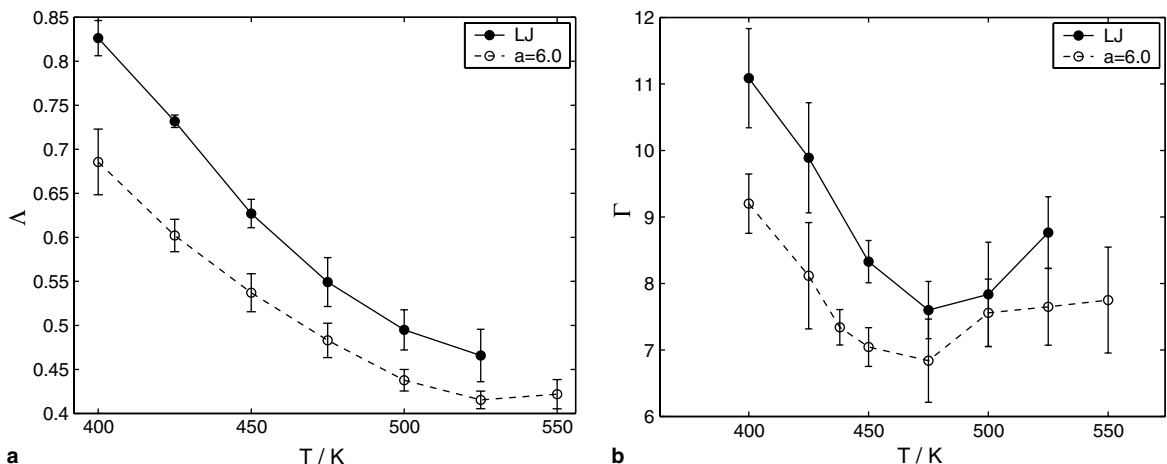

Fig. 8. Temperature dependence of (a) Λ and (b) Γ for the Lennard–Jones potential with $\varepsilon = 5.0\%$ (filled circles) and the Morse $a = 6.0$ potential with $\varepsilon = 6.5\%$ (open circles).
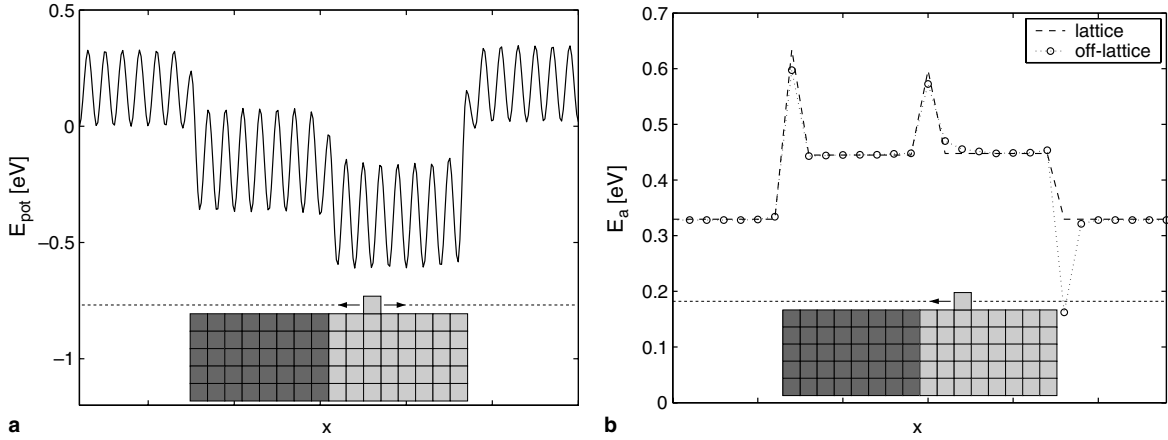
Fig. 9. (a) Sketch of the potential energy for a B particle (light gray) diffusing along the dashed line parallel to the step edge of the small A–B cluster. The values correspond to the Lennard–Jones potential with $\varepsilon = 4\%$. (b) Diffusion barriers for leftward jumps of the B particle from (a). The panel shows values obtained from the off-lattice model (open circles) and as used in the lattice gas approximation (dashed line) discussed in Section 3.1.

simplifying framework. Clearly, strain effects cannot be taken into account explicitly in a pre-defined lattice of possible adatom sites with fixed distances.

3. Lattice description

3.1. Lattice gas simulation model

In our lattice gas model, two adsorbate species A and B grow on a square substrate S with 150×150 adsorption sites. Unlike the off-lattice model where a particle interacts with all particles within the range of the potential, A and B particles interact now only with their lateral nearest neighbors through attractive two-particle interactions with the energy parameters E^{AA}, E^{BB} and E^{AB}. Here, E^{AA}, E^{BB} denote the binding of two A-particles or two B-particles, respectively, and E^{AB} represents the interaction of an A-particle with a B-particle. The total energy of the system can then be written as

$$H = -E^{AA} n^{AA} - E^{BB} n^{BB} - E^{AB} n^{AB} + \mu^A n^A + \mu^B n^B, \tag{10}$$

where n^A, n^B denote the number of A and B particles, and n^{AA}, n^{BB}, n^{AB} count the number of A–A,

B–B and A–B bonds, respectively. The binding of adsorbate particles to the substrate is represented by the effective chemical potentials μ^A and μ^B. Diffusion of adatoms on the surface is described by thermally activated nearest-neighbor hopping processes with Arrhenius rates $R_i = \nu \exp(-E_{a,i}/k_B T)$, where we use again $\nu = 10^{12} \text{ s}^{-1}$ as common attempt frequency. The temperature T is set to 500 K.

A diffusion event i which leads from the starting (s) to the final (f) configuration is modeled using Kawasaki type energy barriers [23] with the activation energy

$$E_{a,i} = \max\{B_{s,i}, B_{f,i} + \Delta H_i\}. \tag{11}$$

Here, ΔH_i denotes the total energy change caused by the diffusion event i which in turn is given by Eq. (10). In general, the diffusion barriers $B_{s,i}$ and $B_{f,i}$ may depend on the type of the diffusing particle as well as the starting and final configuration of the system.

In order to obtain a general insight into the behavior of the model, we consider first a simplified version of our model where A and B particles are treated in a symmetric way, and where the inter-species binding energy is the key characteristics. In Section 3.3, we will use a modified parameter set in order to achieve a comparison between lattice and off-lattice simulations.

3.2. Symmetric treatment of adsorbate species

In this section, we assume that all barriers $B_{s,i}$, $B_{f,i}$ in Eq. (11) are equal, i.e., $B_{s,i} = B_{f,i} = B_0$ for all i. Also, the strength of A–A and B–B bonds will be the same: $E^{AA} = E^{BB} = E^0$. The model is governed by the interaction E^{AB} between A and B particles which is assumed to be weaker than between two particles of the same type: $E^{AB} < E^0$, following the hypothesis in [8]. This has two main implications for a particle diffusing along the step edge of an A–B cluster as the one depicted in Fig. 9. First, the particle is facing an enhanced diffusion barrier when crossing a domain wall. For example, a B particle faces a diffusion barrier $B^0 + E^0 - E^{AB} > B^0$ when it attempts to cross the A–B interface coming from the B side where it is bound more strongly (note, that for the reverse jump, the barrier is B^0), cf. Fig. 9(b). The same happens to an A particle which tries to cross the interface coming from the A side. Thus, A and B particles diffusing along step edges are likely to be reflected at A–B interfaces. Second, the activation energy for detachment of a particle of A or B type from a step edge made up of the opposite type is lower than that for detachment from a step edge of the same type. The two effects combined reflect basically the influence of a weaker A–B interaction in the off-lattice simulations, disregarding though all influences of strain or long range interactions.

To investigate the influence of the binding energy E^{AB}, we fix $B^0 = 0.37$ eV and $E^0 = 0.51$ eV. This reproduces roughly the homoepitaxy ($\varepsilon = 0$) barriers for diffusion on planar substrate and

detachment from an island edge as measured in the off-lattice simulations. E^{AB} is varied between $0.31E^0$ and $0.71E^0$. Following the off-lattice simulation, in all simulation runs the deposition rate for both types of particles is set to 5×10^{-3} ML s^{-1} resulting in an overall deposition rate of $R_d = 10^{-2}$ ML s^{-1}. When the total adsorbate coverage has reached 0.5 ML the simulation is halted.

Fig. 10(a)–(c) shows exemplary configurations obtained at the end of simulation runs for different values of the binding energy E^{AB}. For all values of E^{AB} one observes compact island shapes with the island boundaries roughly parallel to the lattice directions. The weaker binding energy between A and B particles leads to an aggregation of particles of the same type in clusters which can be characterized as stripes. While for the higher value of E^{AB} these stripes are rather thin and show a considerable degree of irregular intermixing for lower values of E^{AB} the stripes are both much thicker and there is a tendency for them to stretch outwards. One also sees that at a certain stage of the island growth a stripe of one particle type may become wide enough for particles of the other type to form a stable nucleus within this stripe, thus leading to a branch-like structure. Similar interplay between growth kinetics and phase ordering has been observed in a simple model with line geometry [25].

The occurrence of the stripe-like structures and the branching under non-equilibrium conditions must be attributed to the kinetic segregation of A and B particles. From thermodynamic considerations one expects more or less complete separation of both particle types for not too high
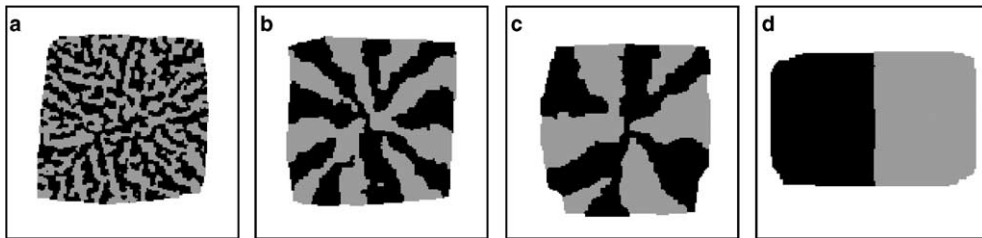

Fig. 10. Lattice gas simulations with symmetric treatment of A and B particles. Island configurations obtained under non-equilibrium growth with $T = 500$ K and $E^0 = 0.51$ eV for $E^{AB} = 0.71E^0, 0.51E^0, 0.47E^0$ (a)–(c). (d) System configuration obtained after $t = 3 \times 10^4$ s of equilibrium simulation with $T = 500$ K, $E^0 = 0.51$ eV and $E^{AB} = 0.26$ eV. The system size is 150×150 and the total coverage is $\Theta = 0.5$ ML.

temperatures and not too large values of E^{AB}. We have tested this assumption by performing canonical equilibrium simulations with fixed adsorbate coverages $n^A/n = n^B/n = 0.25$ ($n = n^A + n^B$) and a random distribution of particles as initial condition. Similar to the off-lattice equilibrium simulations (Section 2.2) we apply a non-local dynamics where in each step an A or B particle from site i may jump to *any* vacant lattice site j.

Fig. 10(d) shows a typical system configuration for $E^{AB} = 0.26$ eV and $T = 500$ K obtained after 3×10^4 s simulated time which confirms that A and B particles separate and due to the attractive binding energy E^{AB} form a single rectangular island consisting of one A and one B region. Note that the interface between the A and the B region is not perfectly straight and the island edges are rounded, in accordance with theoretical calculations which yield $T_R = 0$ as roughening temperature of two-dimensional crystals [26]. Similar results are obtained for various values of E^{AB} and temperature T.

We conclude from our lattice gas simulations, that the step edge barrier indeed gives reason for stripe formation. The equilibrium simulations show that the formation of stripes can be traced back to the kinetic segregation of A and B particles under non-equilibrium growth conditions. The width of the stripes can be controlled by adjusting the binding energy between A and B particles. However as Fig. 10 shows neither asymmetries between A and B clusters nor ramification of the islands is observed here. This is not surprising since A and B particles were treated in a symmetric way, whereas in the off-lattice simulations the different

sign of the misfits causes different diffusion barriers for A and B particles. For example, the substrate diffusion of the B particles with positive misfit is always faster than that of the A particles with negative misfit [16,13,18]. Furthermore in the off-lattice method the barriers for edge diffusion are higher than the substrate diffusion barriers. This could also give rise to a ramified island morphology.

3.3. Comparison of lattice and off-lattice formulation

To account for basic differences of the two particle types in our lattice gas model we now use a modified parameter set which is fitted to reproduce the barriers of characteristic diffusion processes in the off-lattice model. The question is whether a simple misfit dependence of the diffusion barriers could lead to the observed results (e.g., island ramification) within such an enhanced lattice gas model.

Therefore, we extract the barriers for free diffusion on the substrate as well as averaged values for edge diffusion and detachment for a *fixed* island size (see also Fig. 9) as a function of the misfit. These barriers are then used to determine E^{AA}, E^{BB} and E^{AB} as well as the $B_{s,i}$ and $B_{f,i}$ for the different diffusion processes (cf. Eq. (11)). Thus, the modified lattice model incorporates the basic misfit dependence of the diffusion barriers. However, effects of the long range interaction, like the reduced barrier for jumps towards an island (cf. Fig. 9) still have to be neglected here.

Fig. 11 shows a comparison between the lattice model and the off-lattice simulation for the LJ
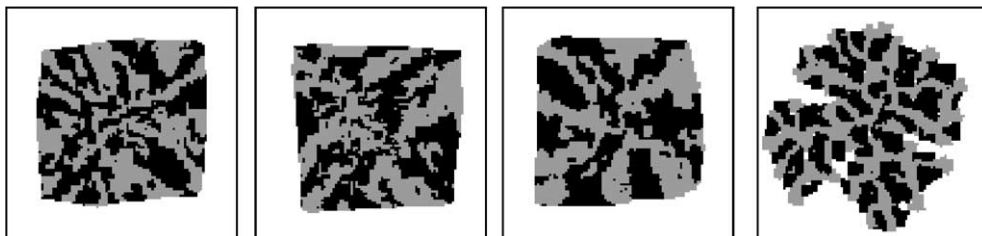

Fig. 11. Comparison of snapshots for the enhanced lattice and the off-lattice model in the case of the Lennard–Jones potential. The panels show (from left to right) lattice/off-lattice results for $\varepsilon = 0$ and lattice/off-lattice results for $\varepsilon = 5\%$. B particles appear in light gray.

potential. Similar results are obtained by fitting the parameters of the lattice gas model to the barriers obtained for the Morse potential. As expected, the islands for both models look very much alike in the case of zero misfit. However, for $\varepsilon = 5\%$ lattice and off-lattice results seem to have little in common. In the case of the lattice model, the separation of A and B regions is more pronounced as for $\varepsilon = 0$ but neither size limitation of the stripes nor island ramification is observable here. On the other hand, asymmetry of the particle species and island ramification are clearly noticeable in the off-lattice configurations. To quantify our observations we have measured the ramification Γ for both lattice and off-lattice simulation results. Fig. 12 shows Γ for various values of the misfit ε. For $\varepsilon = 0$ the islands are roughly quadratic in both types of simulations and thus the curves coincide at $\Gamma \approx 4$. With increasing misfit the islands in the off-lattice simulations become more and more ramified leading to a significant increase of Γ for $\varepsilon > 3\%$. For the lattice simulations though Γ remains constant, i.e., no ramification is observed.

From additional off-lattice simulations, where the reduced barrier for jumps towards an island is suppressed we find that the resulting islands

are less ramified whereas the width of the B branches remains unchanged [13]. The reduced island ramification can be traced back to a higher mobility of the particles: once a particle detaches from an island it has the same probability for jumps towards the island as away from it. The capturing of diffusing adatoms by islands is therefore less pronounced and the particles are more uniformly distributed around the island [13].

These examinations clearly demonstrate that species-dependent diffusion barriers at edges alone are not sufficient to explain the width restriction of the B branches or the ramification of the islands with increasing misfit. Actually, further non-local effects like e.g., the above mentioned adatom capturing play a decisive role. Our enhanced lattice gas model with fitted diffusion barriers thus lacks important features observed in both experiment and off-lattice simulations.

4. Summary and discussion

We have studied two-component pattern formation and island shape ramification in a ternary material system: an adlayer composed of two immiscible components A and B deposited on a substrate S of intermediate lattice spacing. We have developed and studied atomistic models in order to investigate different mechanisms of pattern formation suggested in the literature on the atomistic level. We have compared results obtained with an off-lattice model (with different interaction potentials), and a lattice gas model (with different parameterizations). In all considered models, the inter-species binding is weaker than the binding between species of the same kind. In the off-lattice case the explicit incorporation of adsorbate misfits is possible whereas in the lattice gas description, this feature can be taken into account only indirectly by a modification of the parameters. The combination of both types of models has enabled us to assess the role of the two main mechanisms considered as the driving force of stripe formation: strain relaxation and kinetic segregation of the elements. We have performed both equilibrium and non-equilibrium simulations for the two different model types.
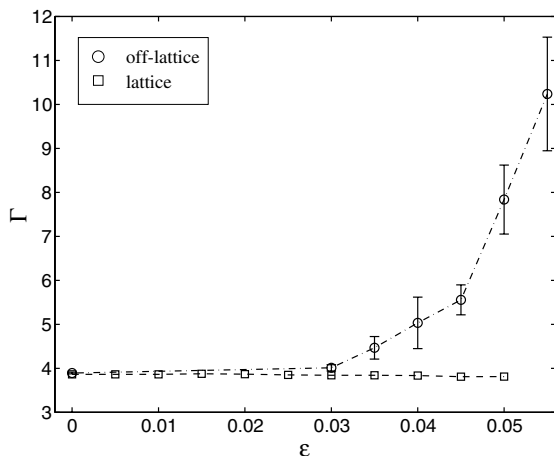

Fig. 12. Island-ramification for lattice and off-lattice simulations. Each value is obtained by averaging over ten independent simulation runs. For the off-lattice simulations errorbars are given by the standard deviation. For the lattice simulations errorbars are smaller than the symbols.

Equilibrium simulations using the off-lattice model have been performed for a completely filled monolayer. The results have shown that the adsorbate materials segregate and form nanoscale stripes with straight boundaries and a stable well-defined width. The stripe width decreases with increasing relative misfits and with increasing inter-species binding energy. Our results indicate also that the stripe width changes with the concentration. The B particles (positive misfit) form thinner stripes at high B concentration than the A particles (negative misfit) at high A concentration. We have observed very similar behavior for different pair-potentials (Lennard–Jones and Morse potential).

The situation is different in the case of equilibrium simulations using the lattice gas model. Here, the system undergoes a complete phase separation with a temperature dependent time of separation. Hence, no stripe structure is formed in the long time limit.

Under non-equilibrium conditions, we have studied the growth of an isolated island. In the off-lattice simulations we have observed the formation of highly ramified monolayer islands with a vein structure similar to that observed in experiments [8]. A pronounced asymmetry is found in the sense that the bigger B particles form a backbone of ramified branches, with the smaller A particles filling in the gaps. While the shape of mixed A–B islands is ramified, we have observed that islands composed of only A or B particles have regular square shape. This agrees with experimental observations [8]. The island ramification has been observed for different interaction potentials. Our results indicate that the ramification of two-component islands is not an artefact of low temperature but the result of chemically induced step edge barriers in combination with the effects of strain.

We have studied quantitatively the dependence of island shape and composition on the misfit and on the temperature. The increase of the misfit causes an increasing ramification, and the increase of the temperature yields wider and more regular stripes. Our results confirm that there is a correlation between the width of the stripes and the smoothness of island edges.

With the help of a simple version of the lattice model in which the inter-species binding energy E^{AB} is the only relevant parameter, we have demonstrated that a chemically induced step edge diffusion barrier is sufficient to cause the formation of structures with alternating stripes. Here, the stripe formation is a purely kinetic effect. The stripe width is selected by a balance of different kinetic rates and can be tuned by E^{AB}. We have observed that the interface of the stripes is rather rough. Moreover, the observed island shapes are regular in contrast to the simultaneous observation of vein structures and dendritic growth in experiment [8] and our off-lattice simulations.

In order to rule out the possibility that the absence of island ramification in the lattice model is merely caused by the oversimplified symmetric treatment of A and B particles we have constructed and studied a modified lattice model in which we have tried to represent the features, i.e., energy barriers, of the off-lattice model as faithful as possible. Nevertheless, the modified model also fails to reproduce the ramification observed in the off-lattice simulations.

A more successful lattice based simulation would have to incorporate non-local effects. Diffusion barriers can depend on quite large neighborhoods in the off-lattice model. For instance, barriers for diffusion along an island edge should depend explicitly on the island size and composition. The above mentioned breaking up of pure B clusters at a characteristic size indicates that the misfit yields island size dependent barriers for attachment or detachment. Such effective long-range interactions can be mediated through elastic deformation of the substrate, for instance. Clearly, an explicit incorporation of cluster size dependent barriers is beyond the scope of a simple lattice gas model and would destroy its conceptional advantages. Alternative routes, e.g., the evaluation of the strain energy for a given lattice configuration, have been suggested and used in the literature, see for instance [31].

For the sake of computational benefits the off-lattice model was formulated for the simple cubic lattice and simple pair-potentials. Nevertheless, we believe that these simplifications do not affect our qualitative conclusions. The model can be

modified and extended in different ways to study specific questions. In order to obtain a closer comparison with experiments on fcc(1 1 1) or fcc(1 1 0) surfaces one needs to change the geometry which implies a more complex evaluation of different possible movements of an atom. Furthermore, additional processes have to be considered if one aims at the study of multilayer growth. Finally, a more realistic description of specific materials requires the use of more sophisticated many-body-potentials as, e.g., tight-binding RGL (Rosato–Guillope–Legrand) potentials [32].

5. Conclusion

Our results have confirmed that both microscopic mechanisms, strain relaxation *and* kinetic segregation, are indeed relevant and crucial for the explanation of essential features observed in experiments, and that the experimental findings cannot be explained completely using only one of them. An equilibrium system with non-zero misfits but otherwise equivalent particle species displays a checkerboard-like mixing of species without the formation of stripes in the whole range of considered misfits. On the other hand, a system with zero misfits and different interactions shows stripe formation but no stable pattern is selected. The system configurations display segregation into domains with a characteristic length controlled only by fluctuations which become very large under close-to-equilibrium conditions. Moreover, islands growing far-from-equilibrium lack the characteristic ramification and asymmetry of material species.

The interplay of, both, different energy barriers and misfit induced strain effects together with the effect of kinetics is needed to explain experimental observations qualitatively. The presented off-lattice model with non-zero misfits and inter-species interactions allowed us to reproduce and quantitatively study the stripe formation as well as the island ramification in the segregation regime.

The comparison of results obtained with the off-lattice and the lattice model show that the presence of chemically induced step edge diffusion barriers at A–B interfaces is sufficient for stripe formation. However, the origin of island edge ramification is

more complex. Ramification was not observed in our lattice model. A satisfactory treatment of this phenomenon within the framework of a lattice gas model will only be possible if the model incorporates effectively long-range elastic interactions.

The presented off-lattice model and its modifications allow also for the study of related problems appearing in ternary systems. For instance, it is an interesting open question, whether the model displays the concentration dependent competition between alloying and dislocation formation in island growth, which has been reported for CoAg/Ru(0 0 0 1) [5]. A case of particular interest is that of an anisotropic substrate which favors the self-assembly of aligned stripes [4]. Such nanostructures exhibit anomalous magnetic properties [33] which are expected to be relevant in the development of novel storage devices.

Acknowledgements

References

[1] M.A. Herman, W. Richter, H. Sitter, Epitaxy. Physical Principles and Technical Implementation, Springer, Berlin, 2004.
[2] B.A. Joyce, P.C. Kelires, A.G. Naumovets, D.D. Vvedensky (Eds.), Quantum Dots: Fundamentals, Applications, and Frontiers, NATO Science Series II: Mathematics, Physics and Chemistry, vol. 190, Springer, Berlin, 2005.
[3] R. Plass, N.C. Bartelt, G.L. Kellogg, J. Phys. Condens. Matter 14 (2002) 4227.
[4] E.D. Tober, R.F.C. Farrow, R.F. Marks, G. Witte, K. Kalki, D.D. Chambliss, Phys. Rev. Lett. 81 (1998) 1897.
[5] G.E. Thayer, V. Ozoliņš, A.K. Schmid, N.C. Bartelt, M. Asta, J.J. Hoyt, S. Chiang, R.Q. Hwang, Phys. Rev. Lett. 86 (2001) 660.
[6] M. Kotrla, N.I. Papanicolaou, D.D. Vvedensky, L.T. Wille (Eds.), Atomistic Aspects of Epitaxial Growth, Kluwer, Dordrecht, 2002.
[7] J. Tersoff, Phys. Rev. Lett. 74 (1995) 434.

[8] R.Q. Hwang, Phys. Rev. Lett. 76 (1996) 4757.

[9] R.Q. Hwang, M.C. Bartelt, Chem. Rev. 97 (1997) 1063.

[10] J.L. Stevens, R.Q. Hwang, Phys. Rev. Lett. 74 (1995) 2078.

[11] B. Sadigh, M. Asta, V. Ozoliņš, N.C. Bartelt, A.A. Quong, R.Q. Hwang, Phys. Rev. Lett. 83 (1999) 1379.

[12] A. Schindler, Ph.D. thesis, Universität Duisburg, 1999.

[13] F. Much, PhD thesis, Universität Würzburg, 2003, arXiv:cond-mat/0410456.

[14] F. Much, M. Ahr, M. Biehl, W. Kinzel, Europhys. Lett. 56 (2001) 791.

[15] F. Much, M. Ahr, M. Biehl, W. Kinzel, Comput. Phys. Commun. 147 (2002) 226.

[16] F. Much, M. Biehl, Europhys. Lett. 63 (2003) 14.

[17] N.W. Ashcroft, N.D. Mermin, Solid State Physics, Saunders College Publishing, Philadelphia, 1976.

[18] M. Schroeder, D.E. Wolf, Surf. Sci. 375 (1997) 129.

[19] O.S. Trushin, M. Kotrla, F. Máca, Surf. Sci. 389 (1997) 55.

[20] F. Máca, M. Kotrla, O.S. Trushin, Vacuum 54 (1999) 113.

[21] B.D. Yu, M. Scheffler, Phys. Rev. B 56 (1997) 15569.

[22] G.L. Kellog, P.J. Feibelman, Phys. Rev. Lett. 64 (1990) 3143.

[23] M.E.J. Newman, G.T. Barkema, Monte Carlo Methods in Statistical Physics, Oxford University Press, Oxford, 1999.

[24] M. Ahr, M. Biehl, Surf. Sci. 505 (2002) 124.

[25] M. Kotrla, M. Předota, Europhys. Lett. 39 (1997) 251.

[26] A. Pimpinelli, J. Villain, Physics of Crystal Growth, Cambridge University Press, Cambridge, 1998.

[27] B.D. Krack, V. Ozoliņš, M. Asta, I. Daruka, Phys. Rev. Lett. 88 (2002) 186101.

[28] G.T. Barkema, N. Mousseau, Phys. Rev. Lett. 77 (1996) 4358.

[29] N. Mousseau, G.T. Barkema, Phys. Rev. E 57 (1998) 2419.

[30] B. Müller, L. Nedelmann, B. Fischer, H. Brune, J.V. Barth, K. Kern, Phys. Rev. Lett. 80 (1998) 2642.

[31] M. Meixner, E. Schöll, V.A. Shchukin, D. Bimberg, Phys. Rev. Lett. 87 (2001) 236101.

[32] F. Cleri, V. Rosato, Phys. Rev. B 48 (1993) 22.

[33] E.D. Tober, R.F. Marks, D.D. Chambliss, K.P. Roche, F.M. Toney, A.J. Kellock, R.F.C. Farrow, Appl. Phys. Lett. 77 (2000) 2728.